ACS Biomaterials SCIENCE & ENGINEERING

pubs.acs.org/journal/abseba

Article

Label-Free Electrochemical Detection of the Cancer Biomarker Platelet-Derived Growth Factor Receptor in Human Serum and Cancer Cells

Chandrababu Rejeeth,* Alok Sharma, Soundarapandian Kannan, Raju Suresh Kumar, Abdulrahman I. Almansour, Natarajan Arumugam, and Samson Afewerki

Cite This: *ACS Biomater. Sci. Eng.* 2022, 8, 826−833

Read Online

ACCESS | Metrics & More | Article Recommendations | Supporting Information

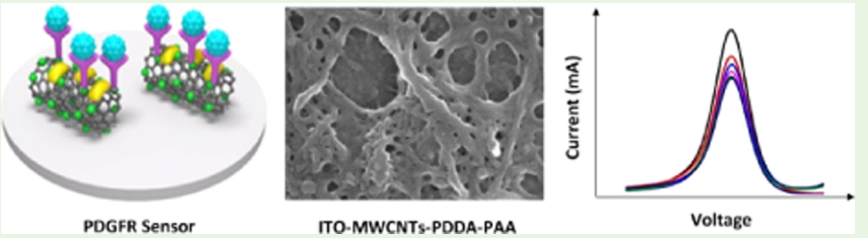

ABSTRACT: Overexpression of the platelet-derived growth factor receptor (PDGFR) was already associated with the loss of p53 function as cancer progresses in lung, breast, and cervical cancers. Cancer biomarker detection has faced challenges and barriers due to various limitations, including a high limit of detection, low sensitivity, time-consuming techniques, and expensive equipment. Hence, the present investigation is designed to develop a cost-effective novel biosensor based on a charge-based affinity bait molecule to detect the PDGFR, thus overcoming the limitations and challenges with an immune technique based on antigen−antibody interactions. We employed EDC−NHS coupling between poly (diallyl dimethylammonium chloride) and poly(acrylic acid) to attach the multiwall carbon nanotube surface. As a result, we performed electrochemical PDGFR conversion sensing with a dynamic range of 1−10,000 ng/mL and a detection limit of 1.5 pg/mL, which is comparable to the best current results. The biosensor also displayed good selectivity, 2.51% repeatability (RSD, n = 5), and 30 days of stability. Our study provides a pathway for the design of diagnostic interfaces in biosystems, as well as the emergence of new sensor types based on ligand−receptor interactions.

KEYWORDS: *label-free, PDGFR, biosensors, electrochemistry, biomarker*

1. INTRODUCTION

During the last decade, cancer biomarker detection has receivedgreat attention in the early treatment and diagnosis of cancer and related diseases.[1,2] In particular, the findings of convincing biomarker proteins in serum (such as the platelet-derived growth factor receptor, PDGFR) exhibited an effectual aspect with high affinity and precision in the diagnosis and prognosis of the disease.[3] Simultaneously, in real-case biosamples, recognized biomarker detection is still challenging due to lower biomarker concentrations and higher biosystem complexity.[1,4] Up to the present time, it is consistently in demand to build a novel stage of biomarker recognition for practical applications. Currently, in particular, in patient care testing, biosensors have been developed as a vital novel tool in clinical medication.[5,6] The biosensor technique includes various benefits of conformity from electrochemistry to chemiluminescence, ensuing a highly sensitive, cost-efficient, simple, and uncomplicated instrumentation approach with a realistic finding.[1,7,8]

For the experimental detection of the biomarkers, a charge-based affinity bait molecule is usually a requisite.[6] The traditional classifying approach, such as the immune technique, depends on antigen−antibody interaction that agonizes from (i) a multicomplex and time-consuming process, (ii) low accuracy because of improper measurement due to labeling, (iii) background noise (such as light and temperature), and (iv) the unaffordable cost of antibodies and associated reagents. Considering the above aspects, affinity substance detection and identification with ligand−protein binding is required as a developing optimal of molecule level credit because of its steadiness, stability, and obvious accessibility. For example, specific grouping between poly(acrylic acid)

Received: September 8, 2021
Accepted: November 18, 2021
Published: December 7, 2021

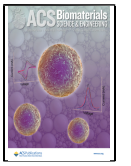

Scheme 1. Schematic Representation of ITO−MWCNTs−PDDA−PAA, Biosensor Fabrication, and Electrochemical Detection of PDGFR

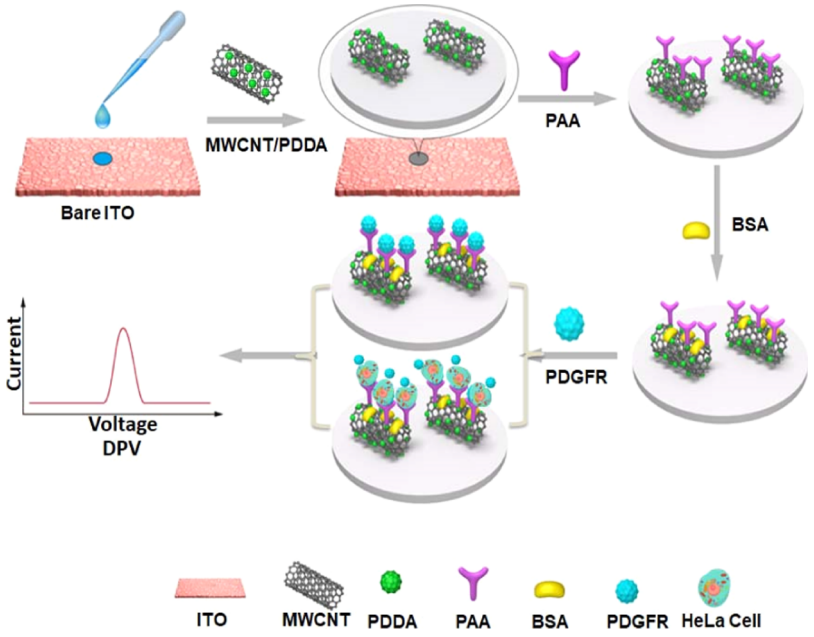

(PAA) and PDGFR can be practical to quantitate and image diseases like cancer, anemia, and other PDGFR-overexpressing systems.[7] Furthermore, only few such kinds of interactions are reported in electrochemistry sensing. However, excellent accuracy, cost-effectiveness, and a label-free technique that avoids the prelabeling process are needed.[8]his novel approach signifies the advanced level device because of its easy handling and specific design for clinical use. Accordingly, a label-free electrochemical detection device is constructed using a ligand−receptor binding approach which contributes to a novel high-efficacy sensor toward disease diagnosis.

The current study describes a novel electrochemical biosensor for detecting the PDGFR via ligand−receptor binding as a detection method (Scheme 1). The biosensor was constructed using a layer-by-layer deposition process. The multiwall carbon nanotubes (MWCNTs) were first functionalized, and then the affinity molecules (1-ethyl-3-(3-dimethylaminopropyl) carbodiimide) were employed to cross-link PAA to indium tin oxide (ITO) by using the EDC−NHS coupling agent. The designed sensor manages a linear range (1−10,000 ng/mL^{-1}) in serum PDGFR detection, and the LOD value reaches 1.5 pg/mL; these are analogous with the best reliable outcome on an electrochemical biosensor. We have also confirmed the detection of HeLa cells, within a limit of 20 cells as in 30 mL of cell suspension, and stability of the sensor for the detection of the biomarker. The current study could be used to improve the platform for PDGFR findings, as well as to develop and design ligand-based approaches for the study of serum biomarkers in label-free diagnostic applications.

2. EXPERIMENTAL PROCEDURES

2.1. Materials. Chemicals such as PAA (M_w = 1800) and poly (diallyl dimethylammonium chloride) PDDA ($M_w \leq$ 100,000) were purchased from Sigma Chemical Co. (Missouri, USA). Bovine serum albumin (BSA) and ITO were obtained from Shenzhen City Science and Technology Co., Ltd. Ethanol was purchased from Beijing Chemical Reagent (Beijing, China). Trypsin (bovine pancreas, TPCK-treated) and recombinant human PDGFR protein were ordered from Abcam Cambridge (Massachusetts, USA). A Milli-Q system purified the water used in all experiments (18.2 MΩ cm) (Millipore, Milford, MA, USA). All of the chemicals obtained were of analytical reagent grade (quality >99%) and were used without further purification. Furthermore, HeLa cells were selected for this study, and they were well maintained on modified media containing high-glucose Dulbecco's modified Eagle's medium supplemented with fetal bovine serum, penicillin, and streptomycin. To extract cells, 1 mL of trypsin (0.25% in PBS, pH 7.2) was added to the flask and kept in a CO_2 incubator for 5 min, after which the cells were rinsed twice with PBS buffer. Using trypan blue and a hemocytometer,[9] the cells were counted under a microscope (Olympus CKX 41). The serum samples were donated by Shanghai Chest Hospital and stored at −80 °C for more experiments.

2.2. Fabrication of the Biosensor. As an electrode, ITO glass was first taken and chopped to the desired size (7.5 mm width and 25 mm height). The ITO glass was ultrasonically treated for 30 min with various dips of 100% alcohol and deionized water. The treated electrodes were rinsed completely with distilled water until no ammonia odor remained and then dried at 100 °C. To make a 1.0 mg/mL PDDA aqueous solution, 0.5 M NaCl was employed. In addition, 1.0 mg of MWCNTs was mixed in 1.0 mL of PDDA solution,[7,10] and the combination was sonicated for 3 h to obtain a homogeneous dark suspension, which was then sonicated for another 15 min well before preparing the MWCNTs−PDDA film. The bare ITO was used to coat the second layer of the MWCNTs−PDDA (15 μL) solution. After air drying, a third layer of 10 μL of PAA assisted with EDC and NHS cross-linker molecules (1 mg/mL)[9] was deposited on the subsequent electrode surface and was kept at room temperature (RT) for about 1 h to produce a stable film. Finally, to avoid nonspecific binding, the electrode was rinsed and incubated in a 1% (wt) BSA solution for 1 h, and the produced biosensors were kept at 4 °C on further application.

2.3. Characterization. The scanning electron microscopy (SEM) study was conducted with a Hitachi S-4800 apparatus (10 kV). After drying at RT, the diced ITO was passed through a conducting resin and observed on a SEM instrument. The contact angle was measured using the OCA 20-assessable/pendant drop experiment (Data Physics), which involved dropping a known amount (5 μL) of water on the paper substrate. The Zeta-Sizer Nano ZS instrument calculates the zeta potential by dispersing the substances in water. The infrared spectum analysis was performed using FT-IR 360 (Nicolet).

https://doi.org/10.1021/acsbiomaterials.1c01135
ACS Biomater. Sci. Eng. 2022, 8, 826−833

An electrochemical workstation (CHI660D, Shanghai, CH Instruments Co., China) was used to conduct the experiment, which included an ITO electrode (working electrode), a Pt wire (counter electrode), and an Ag wire (reference electrode). According to the formula $V_{Ag} = V_{SCE} - 0.07$ V, the Ag wire (reference potential) was calibrated to a saturated calomel electrode (SCE).

2.4. Human Serum Collection. For this study, real-case samples (serum) were collected and stored in tubes according to standard procedures.[11,12] The fabricated biosensor was incubated for 30 min at 37 °C with a series of standard solutions for the recombinant human PDGFR protein at varying concentrations, followed by thorough washing with phosphate buffer. The biosensor is used to detect the concentration of PDGFR in a blood serum sample and a human cervical cancer cell line (HeLa) due to overexpression of PDGFR using the usual PDGFR protein addition method in order to examine the sensor's clinical potential. The biosensor fabrication was performed with the same methods and also incubated in a series of HeLa cells and diluted serum samples with different concentrations; amperometric response detection of standard PDGFR, tumor cell solution, and serum was simultaneously performed by differential pulse voltammetry (DPV) with a pulse amplitude of 50 mV, a pulse width of 50 ms, and a quiet time of 10 s.

2.5. Electrochemical Measurements and ELISA. Electrochemical experiments were conducted using a three-electrode system consisting of a working electrode, a counter electrode, and a reference electrode, namely, a 7.5 × 25 mm ITO electrode (SCST Co., Ltd, China), a Pt wire (SCST Co., Ltd, China), and an Ag/Agcl electrode (SCST Co., Ltd, China) with saturated KCl (SCST Co., Ltd, China). A CHI660E electrochemical workstation was used to perform tests such as DPV and cyclic voltammetry (CV) (CH Instruments Co., Shanghai, China). The electrodes were immersed in a solution of 0.5 mM $K_3[Fe(CN)_6]/K_4[Fe(CN)_6]$ and 0.005 M KCl in a 50 mL electrolyte solution (pH 7.4). The DPV curves were also run with a scan rate of 0.02 V s^{-1}, a sweep segment of 2, a sample interval of 0.001 V, and a quit duration of 2 s from −0.2 to 0.6 V. The enzyme-linked immunosorbent assay (ELISA) kit was supplied by Enzo Life Science, and all the ELISA testing and data analyses were completed according to the standard protocol. The optical density (OD) was determined using a BIOREADER7000, and each OD value was calculated as the average of three observations.

2.6. Statistical Analysis. The statistical analysis in this study was performed using SPSS software (version 24.0.0.0, IBM SPSS Statistics) to calculate the *p*-value using the independent Student's *t*-test for statistical demonstration.[13,14]

3. RESULTS AND DISCUSSION

3.1. Biosensor Construction and Characterization. The layer-by-layer assembly of an electrochemical biosensor is demonstrated in Scheme 1. The presence of ITO nanoparticles revealed by SEM shows surface roughness[4,7] (Figure 1a). After dropping the MWCNTs−PDDA solution, a uniform layer was deposited (Figure 1b). To accommodate PAA-conjugated MWCNTs−PDDA with the help of EDC and NHS cross-linker molecules to generate ITO−MWCNTs−PDDA−PAA as an electrochemical biosensor, the diameter of the carbon nanotubes is significantly enlarged[15,16] (Figure 1c). Furthermore, the biosensor surface morphology was unaffected by the blocking solution BSA[17,18] as demonstrated through the TEM analysis of ITO−MWCNTs and ITO−MWCNTs−PDDA−PAA assembly confirmation showed in TEM (Figure S1a,b). The electrical characteristics of a single MWCNT were investigated using a microscopic composite of linked MWCNTs embedded in a polymer matrix[18] This is the first time that a MWCNTs−PDDA conduction profile has been shown. Only the external sheets are conductive, according to the results. Static contact angle analysis also discloses the hydrophobic and hydrophilic properties of the materials and confirms the measurements. Figure 1d shows the contact angle of bare ITO as 96.4°,[7,19,20] whereas the contact angle of the immobilized MWCNTs−PDDA is 94.2° (Figure 1e)[7,21] because of the hydrophobicity of carboxylated multiwalled carbon nanotubes MWCNTs-COOH and was further reduced to a value of 63.1° due to the hydrophilic nature of the PAA (Figure 1f).[7,22]

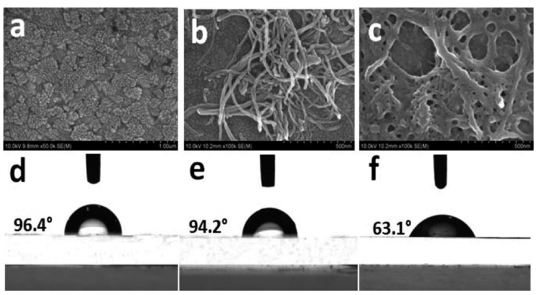

Figure 1. Characterization of materials. Biosensor images from SEM: (a) bare ITO electrode, (b) fabricated electrochemical biosensor (ITO−MWCNTs−PDDA), and (c) biosensor (ITO−MWCNTs−PDDA−PAA−BSA). Contact angle of (d) bare ITO, (e) ITO-MWCNTs−PDDA, and (f) ITO-MWCNTs-PDDA-PAA.

The nano-formulation was confirmed using the Fourier-transform infrared (FTIR) spectrum of MWCNTs (Figure 2a) with peaks at 3293 cm^{-1} for C−H and 1652 cm^{-1} for C=C,[7,23,24] MWCNTs-PDDA with peaks at 1683 cm^{-1} for the primary amine band, NH, and 892 cm^{-1} for vinylidene C−H,[7,25,26] and then MWCNTs-PDDA-PAA with peaks at 1440 cm^{-1} for alkene/alkyl C−H and 1389 cm^{-1} for primary or secondary group, OH[7,26,27] in order to see if functional groups are present after electrode modification. In addition, the zeta potentials of materials are shown in Figure 2b, which are consistent with other characterizations of the layer-by-layer assembly process. The surface modification of electrodes and biosensor fabrication for PDGFR detection without any molecular tags were both effective, according to all the experimental data.

3.2. Optimization of Electrochemical Sensing. The electrodes' electrochemical capability was further proven using DPV and CV curves. Only ITO showed a reduced current peak of 5 mA and 0.2 V on DPV curves (Figure 3a). The current peak increased to 7.8 mA after MWCNTs−PDDA was adjusted, and adding MWCNTs−PDDA−PAA produced a further increase to 10 mA. This could be attributed to carbon nanotubes' high-conductivity characteristics.[28,29] When the electrode was incubated with 1% BSA solution, the current peak was reduced to 8.3 mA (p-value < 0.001). Because BSA has a low electrical conductivity,[7,30,31] this is a distinct possibility. During the entire process of PDGFR biosensor fabrication, the electric conductivity was enhanced fivefold (p-value < 0.001).

The present CV curve responses (Figure 3b) demonstrated the DPV-related consequence. Several parameters were employed to detect PDGFR, including PAA concentration, pH, temperature, and incubation duration (Figure 3c−f). The variation of response current increased up to a maximum of 12.8 mA with saturated adsorption of PAA at 0.4 mg/mL. The current response decreased when the PAA was increased (Figure 3c). The differential response at pH 7.0 was shown to be better than at higher and lower pH values for screening (Figure 3d), and the optimal temperature was found to be 37

https://doi.org/10.1021/acsbiomaterials.1c01135
ACS Biomater. Sci. Eng. 2022, 8, 826−833

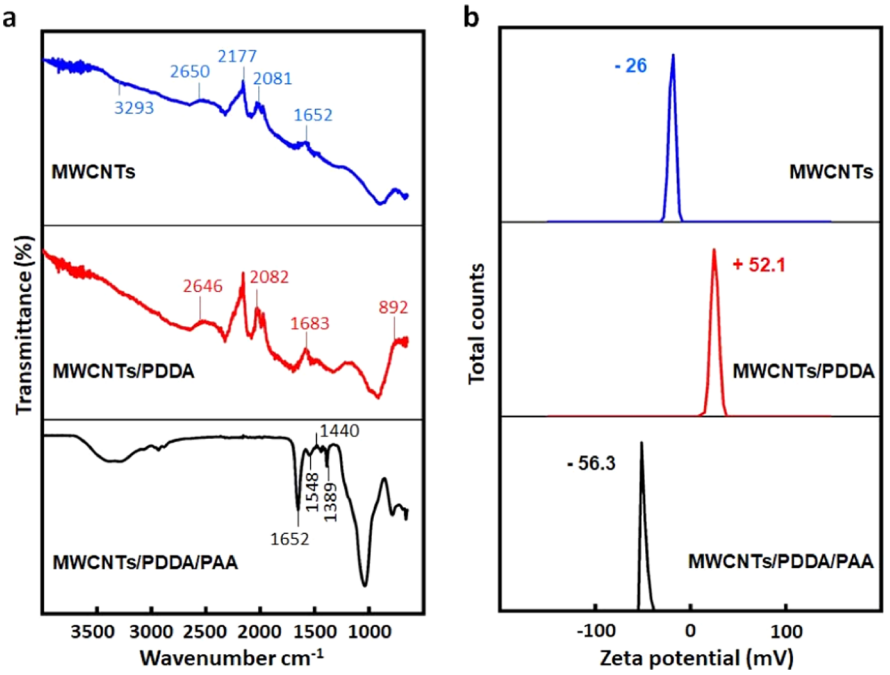

Figure 2. (a) Nano-formulation FTIR analysis, including MWCNTs, MWCNTs−PDDA, and MWCNTs−PDDA−PAA. (b) Zeta potential value of MWCNTs, MWCNTs−PDDA, and MWCNTs−PDDA−PAA.

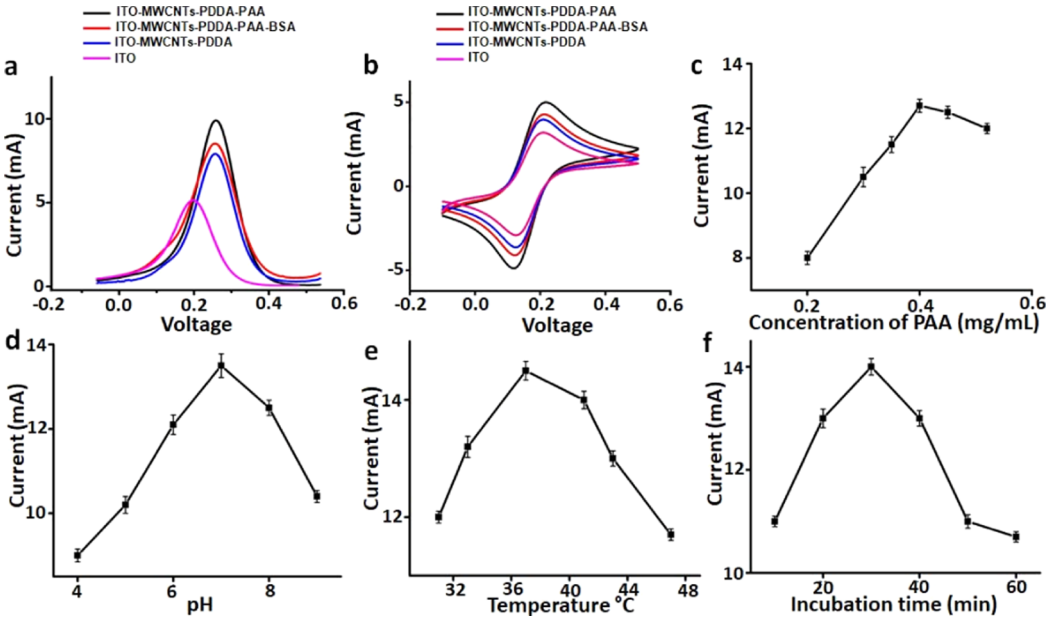

Figure 3. Electrochemical biosensing and optimization are represented in this figure. Typical (a) DPV and (b) CV curves of bare ITO, ITO−MWCNTs−PDDA, ITO−MWCNTs−PDDA−PAA, and ITO−MWCNTs−PDDA−PAA−BSA; under various conditions, the current change of biosensors on the variation of response current peak to 0.25 ng/mL standard PDGFR: (c) PAA concentration, (d) pH value, (e) temperature, and (f) incubation time. All electrochemical experiments were conducted in a 10 mM $K_3[Fe(CN)_6]/K_4[Fe(CN)_6]$ electrolyte, pH 7.4, (the supporting electrolyte was 0.1 M KCl), with error bars in (c−f) representing the standard deviation of three triplicate measurements (n = 3). The DPV was recorded from 500 to 1000 mVwith a pulse amplitude 50 mV, a pulse width of 50 m/s, a scan rate of 20 mV/s, and a quiet time of 2 s.

°C, which was similar to the physiological pH conditions (Figure 3e). Even when the incubation time was increased, the current response remained constant after 30 min (Figure 3f), suggesting that the PAA/PDGFR incubation time may be capped at 30 min. As a result, biosensor enhancements were required for the following application tests. The entire device's construction is depicted in Figure S2.

The DPV curves of various PDGFR concentrations (1−10,000 ng/mL) were accurate and consistent with the optimized conditions. As the PDGFR concentration increased, a negative linear regression with $Y = -0.2178x$ (current response) +5.6 mA and a correlation coefficient of 0.9927 was observed in Figure 4a. The LOD was determined to be 1.5 pg/mL in the regression plot (Figure 4b). Three separate tests were used to calculate the mean and standard deviation of the

https://doi.org/10.1021/acsbiomaterials.1c01135
ACS Biomater. Sci. Eng. 2022, 8, 826−833

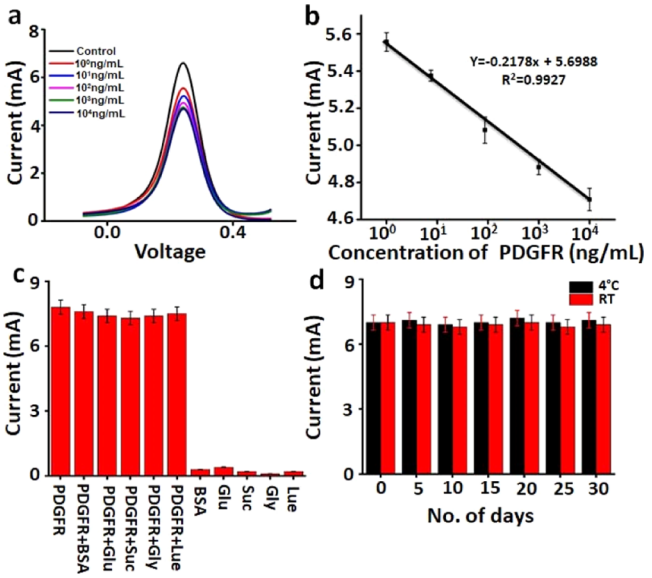

Figure 4. Procedure that involves the detection of PDGFR: (a) typical DPV curves; (b) regression plot of conventional PDGFR solution with varied concentrations ranging from 1 to 10,000 ng/mL^{-1} by the triple independent test; (c) specificity testing of the biosensor using PDGFR, PDGFR + BSA, PDGFR + glucose (Glu), PDGFR + sucrose (Suc), PDGFR + glycine (Gly), PDGFR + leucine (Lue), and BSA, Glu, Suc, Gly, and Lue alone; and (d) the current responses of biosensor after storage at RT and 4 °C for 0−30 days. The standard solution for incubation contained BSA, glucose, sucrose, leucine, and glycine (each at a concentration of 100 ng/mL^{-1}). The standard solutions contained 100 ng/mL^{-1} PDGFR in (c,d).

blank control.[7,32] PDGFR measurements showed high precision, low LOD, and a wide linear spectrum of clinical applications for detecting the PDGFR expression.[33,34] In addition, different PDGFR dilutions in human serum were observed (10, 10^1, 10^2, 10^3, 10^4, and 10^5-fold). As the serum is diluted, the current peak values could increase (Figure S3). Standard PDGFR solutions were investigated using ELISA, demonstrating the electrochemical biosensor's benefits even further. The concentration of PDGFR and optical density at 450 nm (OD 450) showed a polynomial relationship, with an LOD of 42.3 ng/mL^{-1}, according to the regression plot (Figure S4). In comparison to ELISA, the biosensor provided a number of advantages, including (i) a broad linear range and low LOD; (ii) minimal time required (electrochemical biosensor: only ≈1 min for a single DPV curve and ≈35 min for incubation and DPV measurements three times, whereas ELISA method takes ≈100 min); and (iii) a lower cost of only 0.031 $ per biosensor, without labor costs, including the bare ITO electrode (0.022 $ each) and additional chemicals (0.0062 $ for one fabricated electrode), allowing for large-scale applications. The PDGFR biosensor reproducibility, specificity, and stability were all confirmed in the presence of the biosensor. The detection of current change with limited PDGFR concentration is the most significant achievement. It was determined using combined results from PDGFR and other molecules, as well as the biosensor's excellent selectivity (Figure 4c). The current standard solution peaks are also repeatable, with only a (5%) variance, showing strong interbiosensor repeatability (Figure S5). The obtained results, on the other hand, were found to have a high level of reproducibility when compared to PDGFR sensing. Under the same experimental conditions, the repeatability of the proposed sensor was tested using 30 electrodes (see Figure S6). This result demonstrates exceptional performance, with a relative standard deviation of 2.51%. The ITO−MWCNTs−PDDA−PAA was further tested for stability under 4 °C and RT storage conditions. The relative current signal of ITO−MWCNTs−PDDA−PAA reduced marginally over 30 days at RT.[4,7] When stored at 4 °C, the biosensor performance is 97%; however, when stored at RT, only 90% is achieved (Figure 4d). In particular, the excellent performance of the biosensor in this work could be comparable to the best current results exhibited in Tables 1 and 2, and the sensor's additional application in serum analysis demonstrated the sensor's potential in clinical diagnostics.

3.3. Detection of PDGFR in Cancer Cells. Further investigation was carried out on a suspension of HeLa cells with a concentration of 10^3 to 10^6 cells/mL (Figure 5a). With a correlation coefficient of 0.9896, the stable linear regression equation for cancer cells was $y - 0.2451x \times \log [\text{cell}_{\text{concentration}}] + 7.6829$, in which the cell concentration increased for cancer cell absorption (Figure 5b). With an S/N of 3, the detection limit for cancer cells was determined to be ∼20 cells/mL. Particularly, the biosensor surface scanning by SEM binding shows the capture of HeLa and PDGFR-overexpressing HeLa cells.[7] Topological-view SEM (Figure 5c) reveals the attachment of HeLa cells (size of ∼10 μm) with wrinkled cellular morphology. In addition, slanting tilted-view SEM at a 45° angle (Figure 5d) revealed that the cancer cells were tightly attached to the ITO−MWCNTs−PDDA−PAA biosensor surface, similar to that of the top view. Previous literature clearly authenticated that PDGFR was found to be overexpressed in cancer tissue, and hence, PDGFR is reported as one among the proteomic cancer biomarkers. Accordingly, in the present investigation, the overexpression of PDGFR in HeLa cells had been evaluated using the newly developed PDGFR biosensor. This study makes it crystal clear that the PDGFR-overexpressing cancer cells have a greater affinity toward the ITO−MWCNTs−PDDA−PAA biosensor. Furthermore, the data in (Figure 5a,b) demonstrate that the current response rapidly decreased in the first 30 min before being leveled out.

Table 1. Proposed Experimental Method Compared to Previous Cancer Cell Detection Reports

parameter	type of cells	linear range (cells mL^{-1})	limit of detection (cells)	refs
closed BPE-ECL	HL-60	6.0×10^2 to 1.0×10^6	18	23
ECL	HeLa	20−1.0×10^4	8	24
ECL	CCRF-CEM	1.0×10^2 to 1.0×10^5	7	25
electrochemical immunoassay	HL-60	1.0×10^3 to 1.0×10^6	40	26
ECL	HL-60	56−5.6×10^6	1	27
EIS	CCRF-CME	1.0×104 to 1.0×10^7	30	28
DPV	HeLa	1.0×10^3 to 1.0×10^6	20	this assay

https://doi.org/10.1021/acsbiomaterials.1c01135
ACS Biomater. Sci. Eng. 2022, 8, 826−833

Table 2. Comparison of the Proposed Method with Previous Electrochemical Biosensors for the Determination of the PDGFR Receptor

method	technique	linear range	LOD	refs
voltammetric	DPV	0.001−10 Nm	0.3 pM	29
voltammetric	CV	0.001−1 nM	0.4 pM	30
voltammetric	DPV	0.005−60 nM	1.7 pM	31
voltammetric	DPV	0.1 pg mL^{-1} to 50 ng mL^{-1}	50 fg mL^{-1}	32
voltammetric	SWV	0.1 pM to 1 nM	52 fM	33
voltammetric	DPV	50−500 ng mL^{-1}	18 pg mL^{-1}	34
voltammetric	DPV	0.5−50 nM	1.5 pM	this assay

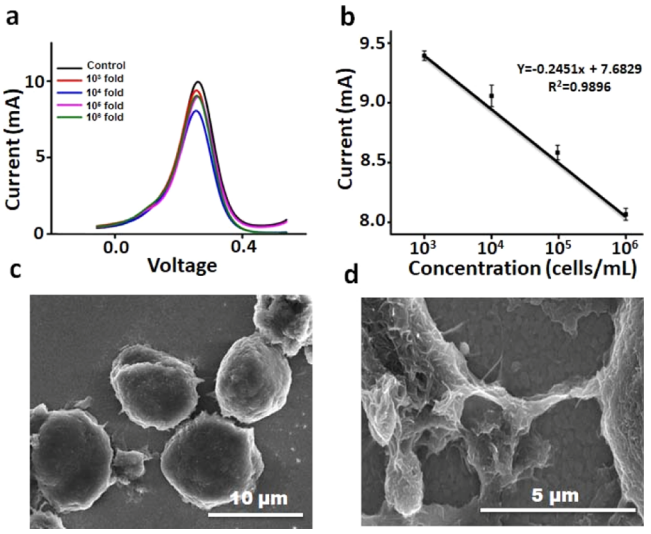

Figure 5. PDGFR cancer cell quantification: (a) PDGFR cancer cell DPV curves (HeLa) with a concentration of 10^3 to 10^6 cells/mL; (b) calibration plot of the response current peak and concentration of cancer cells; and (c) top-view and (d) side-view SEM images of captured cancer cells on the surface of the ITO−MWCNTs−PDDA−PAA biosensor. All electrochemical studies were carried out under optimum conditions in a 10 mM $K_3[Fe(CN)_6/K_4[Fe(CN)_6]$ electrolyte, pH 7.4 (the supporting electrolyte was 0.1 m KCl); error bars in (b) were the standard deviation of three replicate measurements (n = 3). The DPV was recorded from 500 to 100 mV with a pulse amplitude of 50 mV, a pulse width of 50 ms, a scan rate of 20 mV/s, and a quiet time of 2 s.

As a result, for all subsequent incubation processes, the optimum incubation period could be limited to 30 min.

4. CONCLUSIONS

In conclusion, a novel label-free electrochemical biosensor (ITO−MWCNTs−PDDA−PAA) for sensitive detection based on ligand−receptor interaction of PDGFR and PDGFR overexpressing cancer cells (HeLa) and its fabrication were developed. The biosensor demonstrated the following major benefits: (i) label-free capture of PDGFR using the PAA ligand, (ii) MWCNTs−PDDA nanocomposite assemblies increased the biosensor sensitivity, and (iii) the detection of PDGFR in human serum and PDGFR overexpressing cancer cells (HeLa) in a real case. For materials science, a new interface platform will increase the biosensor's efficiency even further. For cost-effective detection in analytical science, electrochemical specific probes are used. For clinical research, the biosensor's application may be limited to real-time testing of specimens where the PDFGR is overexpressed as a biomolecule for various diseases. Overall, the benefits and methods outlined above highlight our approach, which can not only serve as a flexible platform for capturing and detecting unique cancer biomarker proteins but also make electrochemical biosensors more useful in biomedical fields.

■ ASSOCIATED CONTENT

Supporting Information

The Supporting Information is available free of charge at https://pubs.acs.org/doi/10.1021/acsbiomaterials.1c01135.

Additional characterization of materials, TEM, digital images of the three-electrode system, DPV responses of different folds of the serum sample, regression plot by ELISA using standard PDGFR solutions, DPV current peaks, and stability test (PDF)

■ AUTHOR INFORMATION

Corresponding Author

Chandrababu Rejeeth − *School of Biomedical Engineering, Med-X Research Institute, Shanghai Jiao Tong University, Shanghai 200030, PR China; Department of Biochemistry, Periyar University, Salem, Tamil Nadu 636011, India;* orcid.org/0000-0001-8377-8691; Phone: +91 6369283992; Email: crejee@gmail.com

Authors

Alok Sharma − *Department of Pharmacognosy, ISF College of Pharmacy, Moga Punjab 142001, India*

Soundarapandian Kannan − *Division of Cancer Nanomedicine, School of Life Sciences, Periyar University, Salem 636011, India*

Raju Suresh Kumar − *Department of Chemistry, College of Science, King Saud University, Riyadh 11451, Saudi Arabia*

Abdulrahman I. Almansour − *Department of Chemistry, College of Science, King Saud University, Riyadh 11451, Saudi Arabia*

Natarajan Arumugam − *Department of Chemistry, College of Science, King Saud University, Riyadh 11451, Saudi Arabia;* orcid.org/0000-0001-9073-155X

Samson Afewerki − *Division of Engineering in Medicine, Department of Medicine, Brigham and Women's Hospital, Harvard Medical School, Boston, Massachusetts 02115, United States; Division of Health Sciences and Technology, Harvard University—Massachusetts Institute of Technology (MIT), Cambridge, Massachusetts 02139, United States*

Complete contact information is available at: https://pubs.acs.org/10.1021/acsbiomaterials.1c01135

Author Contributions

C.R. envisaged this project and devised the general strategy. The experiments were carried out by C.R. and A.S; C.R., A.S.,

https://doi.org/10.1021/acsbiomaterials.1c01135
ACS Biomater. Sci. Eng. 2022, 8, 826−833

and S.K. examined the data and helped with the materials/device preparation and analytical tests. The article was revised with the assistance of R.S.K and S.A. All authors contributed to the critical discussion and editing of the article, and they all approved the final version.

Notes

The authors declare no competing financial interest.

■ ACKNOWLEDGMENTS

The corresponding authors gratefully acknowledge the Dr. D. S. Kothari Postdoctoral Fellowship, no. F.4-2/2006 (BSR)/BL/19-20/0217 from the University Grants Commission (UGC) of India and Shanghai Jiao Tong University (SJTU), China for providing the necessary facilities. We are thankful to the RUSA fund for SEM facility to Periyar University, Salem, India. The project was supported by Researchers Supporting Project number (RSP-2021/142), King Saud University, Riyadh, Saudi Arabia.

■ REFERENCES

(1) Wu, L.; Qu, X. Cancer biomarker detection: recent achievements and challenges. *Chem. Soc. Rev.* **2015**, *44*, 2963−2997.

(2) Williams, R. M.; Lee, C.; Galassi, T. V.; Harvey, J. D.; Leicher, R.; Sirenko, M.; Dorso, M. A.; Shah, J.; Olvera, N.; Dao, F.; Levine, D. A.; Heller, D. A. Noninvasive ovarian cancer biomarker detection via an optical nanosensor implant. *Sci. Adv.* **2018**, *4*, No. eaaq1090.

(3) Wang, X.; Wu, X.; Zhang, A.; Wang, S.; Hu, C.; Chen, W.; Shen, Y.; Tan, R.; Sun, Y.; Xu, Q. Targeting the PDGF-B/PDGFR-β Interface with Destruxin A5 to Selectively Block PDGF-BB/PDGFR-$\beta\beta$ Signaling and Attenuate Liver Fibrosis. *EBioMedicine* **2016**, *7*, 146−156.

(4) Rejeeth, C.; Pang, X.; Zhang, R.; Xu, W.; Sun, X.; Liu, B.; Lou, J.; Wan, J.; Gu, H.; Yan, W.; Qian, K. Extraction, detection, and profiling of serum biomarkers using designed Fe3O4@SiO2@HA core−shell particles. *Nano Res.* **2018**, *11*, 68−79.

(5) Soleymani, L.; Li, F. Mechanistic Challenges and Advantages of Biosensor Miniaturization into the Nanoscale. *ACS Sens.* **2017**, *2*, 458−467.

(6) Arlett, J. L.; Myers, E. B.; Roukes, M. L. Comparative advantages of mechanical biosensors. *Nat. Nanotechnol.* **2011**, *6*, 203−215.

(7) Zhang, R.; Rejeeth, C.; Xu, W.; Zhu, C.; Liu, X.; Wan, J.; Jiang, M.; Qian, K. Label-Free Electrochemical Sensor for CD44 by Ligand-Protein Interaction. *Anal. Chem.* **2019**, *91*, 7078−7085.

(8) Kylilis, N.; Riangrungroj, P.; Lai, H.-E.; Salema, V.; Fernández, L. Á.; Stan, G.-B. V.; Freemont, P. S.; Polizzi, K. M. Whole-Cell Biosensor with Tunable Limit of Detection Enables Low-Cost Agglutination Assays for Medical Diagnostic Applications. *ACS Sens.* **2019**, *4*, 370−378.

(9) Rejeeth, C.; Vivek, R.; NipunBabu, V.; Sharma, A.; Ding, X.; Qian, K. Cancer nanomedicine: from PDGF targeted drug delivery. *MedChemComm* **2017**, *8*, 2055−2059.

(10) Dag, D.; Guner, S.; Oztop, M. H. Physicochemical mechanisms of different biopolymers' (lysozyme, gum arabic, whey protein, chitosan) adsorption on green tea extract loaded liposomes. *Int. J. Biol. Macromol.* **2019**, *138*, 473−482.

(11) Sun, X.; Huang, L.; Zhang, R.; Xu, W.; Huang, J.; Gurav, D. D.; Vedarethinam, V.; Chen, R.; Lou, J.; Wang, Q.; Wan, J.; Qian, K. Metabolic Fingerprinting on a Plasmonic Gold Chip for Mass Spectrometry Based in Vitro Diagnostics. *ACS Cent. Sci.* **2018**, *4*, 223−229.

(12) Liu, W.; Sun, S.; Huang, Y.; Wang, R.; Xu, J.; Liu, X.; Qian, K. Label-Free Detection of Transferrin Receptor by a Designed Ligand-Protein Sensor. *Chem.—Asian J.* **2020**, *15*, 56−60.

(13) Rejeeth, C.; Vivek, R. Comparison of two silica based nonviral gene therapy vectors for breast carcinoma: evaluation of the p53 delivery system in Balb/c mice. *Artif. Cells, Nanomed., Biotechnol.* **2017**, *45*, 489−494.

(14) Rejeeth, C.; Vivek, R.; Kannan, S. A novel magnetic drug delivery nanocomplex with a cisplatin-conjugated Fe3O4 core and a PEG-functionalized mesoporous silica shell for enhancing cancer drug delivery efficiency. *RSC Adv.* **2015**, *5*, 94534−94538.

(15) Maziukiewicz, D.; Maciejewska, B. M.; Litowczenko, J.; Kościński, M.; Warowicka, A.; Wychowaniec, J. K.; Jurga, S. Designing biocompatible spin-coated multiwall carbon nanotubes-polymer composite coatings. *Surf. Coat. Technol.* **2020**, *385*, 125199.

(16) Lin, Z.-I.; Lou, C.-W.; Pan, Y.-J.; Hsieh, C.-T.; Huang, C.-L.; Huang, C.-H.; Chen, Y.-S.; Lin, J.-H. The effects of MWCNT length on the mechanical, crystallization and electromagnetic interference shielding effectiveness of PP/MWCNT composites. *J. Polym. Res.* **2017**, *24*, 32.

(17) Ji, S.; Lee, M.; Kim, D. Detection of early stage prostate cancer by using a simple carbon nanotube@paper biosensor. *Biosens. Bioelectron.* **2018**, *102*, 345−350.

(18) Gayathri, C. H.; Mayuri, P.; Sankaran, K.; Kumar, A. S. An electrochemical immunosensor for efficient detection of uropathogenic E. coli based on thionine dye immobilized chitosan/functionalized-MWCNT modified electrode. *Biosens. Bioelectron.* **2016**, *82*, 71−77.

(19) Bayoudh, S.; Othmane, A.; Bettaieb, F.; Bakhrouf, A.; Ouada, H. B.; Ponsonnet, L. Quantification of the adhesion free energy between bacteria and hydrophobic and hydrophilic substrata. *Mater. Sci. Eng., C* **2006**, *26*, 300−305.

(20) Zhong, Z.; Zhong, Y.; Liu, C.; Yin, S.; Zhang, W.; Shi, D. Study on the surface wetting properties of treated indium-tin-oxide anodes for polymer electroluminescent devices. *Phys. Status Solidi A* **2003**, *198*, 197−203.

(21) Shao, H.; Zhao, P.; Su, L.; Tian, L.; Zhang, Y.; Sun, Y.; Yue, S.; Xue, W.; Ramakrishna, S.; He, L. Fabrication of carbon nanotube nanocomposites via layer-by-layer assembly and evaluation in biomedical application. *Nanomedicine* **2016**, *11*, 3087−3101.

(22) Qi, Y.; Ma, H.-L.; Du, Z.-H.; Yang, B.; Wu, J.; Wang, R.; Zhang, X.-Q. Hydrophilic and Antibacterial Modification of Poly(lactic acid) Films by γ-ray Irradiation. *ACS Omega* **2019**, *4*, 21439−21445.

(23) Nadafan, M.; Tohidifar, M. R.; Karimi, M.; Malekfar, R.; Khorrami, G. Assessment of the optical and dielectric properties of f-MWCNTs/BaTiO3 nanocomposite ceramics. *Ceram. Int.* **2018**, *44*, 15804−15808.

(24) Duc Chinh, V.; Speranza, G.; Migliaresi, C.; Van Chuc, N.; Minh Tan, V.; Phuong, N.-T. Synthesis of Gold Nanoparticles Decorated with Multiwalled Carbon Nanotubes (Au-MWCNTs) via Cysteaminium Chloride Functionalization. *Sci. Rep.* **2019**, *9*, 5667.

(25) Zhao, Q.; Qian, J.; Zhu, M.; An, Q. Facile fabrication of polyelectrolyte complex/carbon nanotube nanocomposites with improved mechanical properties and ultra-high separation performance. *J. Mater. Chem.* **2009**, *19*, 8732−8740.

(26) Wang, C.; Gong, W.; Lu, X.; Xiang, Y.; Ji, P. Heparin Immobilized on Multiwalled Carbon Nanotubes for Catalytic Conversion of Fructose in Water with High Yield and Selectivity. *ACS Omega* **2019**, *4*, 16808−16815.

(27) Zhou, T.; Wang, M.; He, X.; Qiao, J. Poly(vinyl alcohol)/Poly(diallyldimethylammonium chloride) anion-exchange membrane modified with multiwalled carbon nanotubes for alkaline fuel cells. *J. Materi.* **2019**, *5*, 286−295.

(28) Yun, D.-J.; Hong, K.; Kim, S. h.; Yun, W.-M.; Jang, J.-y.; Kwon, W.-S.; Park, C.-E.; Rhee, S.-W. Multiwall Carbon Nanotube and Poly(3,4-ethylenedioxythiophene): Polystyrene Sulfonate (PEDOT:PSS) Composite Films for Transistor and Inverter Devices. *ACS Appl. Mater. Interfaces* **2011**, *3*, 43−49.

(29) Ko, Y. G.; Do, T. G.; Oh, H. C.; Lee, H. J.; Han, H.-g.; Kim, C. H.; Choi, U. S. Line-patterning of polyaniline coated MWCNT on stepped substrates using DC electric field. *Sci. Rep.* **2014**, *4*, 6656.

(30) Wang, R.; Zhou, X.; Zhu, X.; Yang, C.; Liu, L.; Shi, H. Isoelectric Bovine Serum Albumin: Robust Blocking Agent for Enhanced Performance in Optical-Fiber Based DNA Sensing. *ACS Sens.* **2017**, *2*, 257−262.

https://doi.org/10.1021/acsbiomaterials.1c01135
ACS Biomater. Sci. Eng. 2022, 8, 826−833

(31) Kaushik, A.; Yndart, A.; Kumar, S.; Jayant, R. D.; Vashist, A.; Brown, A. N.; Li, C.-Z.; Nair, M. A sensitive electrochemical immunosensor for label-free detection of Zika-virus protein. *Sci. Rep.* **2018**, *8*, 9700.
(32) Salahandish, R.; Ghaffarinejad, A.; Naghib, S. M.; Majidzadeh-A, K.; Zargartalebi, H.; Sanati-Nezhad, A. Nano-biosensor for highly sensitive detection of HER2 positive breast cancer. *Biosens. Bioelectron.* **2018**, *117*, 104−111.
(33) Razmi, N.; Baradaran, B.; Hejazi, M.; Hasanzadeh, M.; Mosafer, J.; Mokhtarzadeh, A.; de la Guardia, M. Recent advances on aptamer-based biosensors to detection of platelet-derived growth factor. *Biosens. Bioelectron.* **2018**, *113*, 58−71.
(34) Li, Y.; Liu, Z.; Lu, W.; Zhao, M.; Xiao, H.; Hu, T.; Ma, J.; Zheng, Z.; Jia, J.; Wu, H. A label-free electrochemical aptasensor based on the core−shell Cu-MOF@TpBD hybrid nanoarchitecture for the sensitive detection of PDGF-BB. *Analyst* **2021**, *146*, 979−988.

https://doi.org/10.1021/acsbiomaterials.1c01135
ACS Biomater. Sci. Eng. 2022, 8, 826−833